International Journal of Mechanical, Industrial and Aerospace Sciences
ISSN: 2517-9950
Vol:7, No:7, 2013

Combining Molecular Statics with Heat Transfer Finite Difference Method for Analysis of Nanoscale Orthogonal Cutting of Single-Crystal Silicon Temperature Field

Zone-Ching Lin, Meng-Hua Lin, and Ying-Chih Hsu

***Abstract*—**This paper uses quasi-steady molecular statics model and diamond tool to carry out simulation temperature rise of nanoscale orthogonal cutting single-crystal silicon. It further qualitatively analyzes temperature field of silicon workpiece without considering heat transfer and considering heat transfer. This paper supposes that the temperature rise of workpiece is mainly caused by two heat sources: plastic deformation heat and friction heat. Then, this paper develops a theoretical model about production of the plastic deformation heat and friction heat during nanoscale orthogonal cutting. After the increased temperature produced by these two heat sources are added up, the acquired total temperature rise at each atom of the workpiece is substituted in heat transfer finite difference equation to carry out heat transfer and calculates the temperature field in each step and makes related analysis.

***Keywords*—**Quasi-steady molecular statics, Nanoscale orthogonal cutting, Finite difference, Temperature.

I. Introduction

CONCERNING the nanoscale cutting, Shimada [1] used two-dimensional (2D) model and molecular dynamics to conduct dynamic simulation of single-crystal orthogonal cutting and explore the cause of formation of chips. Childs et al. [2] and Belak et al. [3] employed molecular dynamics theory to conduct numerical simulation, but their model still lacked a complete quantitative calculation. Pei et al. [4] indicated that the rake angle of cutting tool had significant influence on formation of chips and workpiece surface. The chips under rake angle -45^{o} would be less because the workpiece has greater plastic deformation. Besides, the chips under rake angle -45^{o} would have greater rebounding. Inamura et al. [5] regarded atoms as nodes, and combined the Morse potential among atoms with the work of atoms in order to overturn finite element method of atomic model. Furthermore, the concept of weight function was imported to induce the relationship among the displacement, strain and stress between atomic model and continuum model, resulting in strain distribution and stress distribution of workpiece. Cai et al. [6] used the same cutting tool radius to explore different cutting depths on silicon workpiece, and make simulative comparison among different cutting depths and radii of cutting tools. They found that the radius of cutting had to be properly small so as for easier cutting. The 2D model of Shimada [7] used molecular dynamics to carry out dynamic simulation of single-crystal silicon orthogonal cutting, and explore the cause of formation of chips. Tanakal and Shimada [8] used different volumes to match with different cutting depths, and different radii and different rake angles of cutting tools to explore the change of ductility and brittleness of silicon material. It was found that production of cracks could be avoided, and the cutting tool with negative rake angle could be effectively applied to ductile cutting. Tang [9] used conic cutting tool at 3nm to simulate cutting of silicon workpiece. M. Cai et al. [10] used round-edge cutting tools with different nose radii to conduct simulation of molecular dynamic cutting of silicon workpiece, and compared the temperatures produced during fabrication by cutting tools with different parameters.

The existing literature used molecular dynamics model to simulate heat source temperature. But this paper develops the use of molecular statics to carry out cutting simulation to calculate temperature rise of plastic deformation heat source and friction rise of friction heat source respectively, and find the temperature field without considering heat transfer. Furthermore, this paper uses heat transfer finite different method to obtain the temperature field with considering heat transfer, and explores the sharp tool and round edge tool would cause effects on production of cutting force and temperature heat source of the material. Using round edge cutting tool and employing the way of molecular statics orthogonal cutting simulation, the paper calculates the temperature field, makes qualitative verification comparison with the molecular dynamics simulation results obtained by M. Cai et al. [10], and analyzes the physical phenomenon.

II. Three Dimensional Quasi-Steady Molecular Statics Nanocutting Model

A. Calculation of Cutting Force

Through molecular statics, this paper finds the quasi-steady force balance equation to calculate the motion displacement of each atom and atoms cannot go through another atom easily to create much deformation, this paper supposes that each feed

Z. C. Lin is with the Department of Mechanical Engineering, National Taiwan University of Science and Technology, 43 Keelung Road, Section 4, Taipei 10672,Taiwan, (phone: +886-2-2737 6455; fax: +886-2-2737 6423; e-mail: zclin@ mail.ntust.edu.tw).

M. H. Lin and Y. C. Hsu are with the Department of Mechanical Engineering, National Taiwan University of Science and Technology, (e-mail: m9803237@ mail.ntust.edu.tw, d9203205@mail.ntust.edu.tw, respectively).

does not exceed a distance of 1/2 lattice constant during searching the most suitable position of force balance deformation displacement.

The quasi-steady molecular statics nanocutting model of this paper uses the adopts Morse potential energy of two-body potential energy as the basis for calculation of the action force between molecules. For the Morse potential energy function [11], when the distance between two atoms is greater than a certain distance, the action force between atoms will decrease rapidly. Therefore, it defines the distance cut-off radius r_c, and when the distance exceeds rc, the action force is very small so it does not need to be calculated. In this way, the calculation can be tremendously simplified. Therefore, the Morse potential energy of the distance between two atoms inside r_c and outside r_c can be further expressed as (1):

$$\begin{cases} \Phi(r_{ij}) = D\left\{e^{-2\alpha(r_{ij}-r_0)} - 2e^{-\alpha(r_{ij}-r_0)}\right\} & r \le r_c \\ \Phi(r_{ij}) \cong 0 & r \ge r_c \end{cases} \quad (1)$$

where D is binding energy, α is material parameter, r_{ij} is distance between two atoms and r_0 is equilibrium distance.

According to the Morse potential used by this paper, the action force between two atoms can be expressed as (2):

$$F(r_{ij}) = -\frac{\partial \Phi(r_{ij})}{\partial (r_{ij})} = 2D\alpha\left\{e^{-2\alpha(r_{ij}-r_0)} - 2e^{-\alpha(r_{ij}-r_0)}\right\} \quad (2)$$

when $r_{ij}=r_0$, the action force between atoms is just situated at a balance between attraction force and repulsive force. Both the cutter and workpiece material are at the situation of no action force. When $r_{ij}<r_c$, the diamond cutter and silicon material will produce action force. As known from (2), when r_{ij} value is smaller, the action force produced between two atoms will be greater, making the silicon material of workpiece pushed away from the original balanced position by the action force. As the step of cutter moves forward, the so-called chip phenomenon is formed.

By using (2), it can infer that the action force between two atoms can be expressed as (3):

$$\vec{F}_i = \sum_{i=1}^{n} \vec{F}_{ij}(r_{ij}) \quad (3)$$

i: a number given to the carbon atom of cutter.
j: a number given to the silicon atom in material.
n: number of silicon atoms.
r_{ij}*:* distance between two atoms.

The action force between two atoms acquired from (3) can be further divided into the components of force in three axes, $\vec{F}x$, $\vec{F}y$ and $\vec{F}z$, as shown in (4):

$$\vec{F}_i = \vec{F}x_i + \vec{F}y_i + \vec{F}z_i \quad (4)$$

$\vec{F}x_i$: component of force of the action force in X direction

$\vec{F}y_i$: component of force of the action force in Y direction

$\vec{F}z_i$: component of force of the action force in Z direction

Of course, after cutting has proceeded for a certain period, there is not just one silicon workpiece atom influenced by the Morse force of the diamond cutter. Hence, the Morse force vector of each silicon atom of the silicon workpiece being affected by the Morse force of diamond cutter after having moved to the new position, as well as the Morse force of other silicon atoms inside the cut-off radius acted on by each atom after moving to the new position are used in sequential order to find the sum of Morse force vector of each silicon atom. The sum of Morse force vector are further resolved as the Morse force component F_X in the X direction as well as the Morse force component F_Y in Y direction and F_Z in Z direction. As mentioned above, let the sum of the Morse force components in the X, Y and the Z directions be zero respectively. Then the force equilibrium equation of the quasi-steady molecular statics nanocutting model is formed, as shown in (5).

$$\begin{cases} F_X = \sum_{i=1}^{m} \vec{F}_{ix}(r_{ij}) = \sum_{i=1}^{m}\sum_{j=1}^{n} F_x(r_{ij}) = 0 \\ F_Y = \sum_{i=1}^{m} \vec{F}_{iy}(r_{ij}) = \sum_{i=1}^{m}\sum_{j=1}^{n} F_y(r_{ij}) = 0 \\ F_Z = \sum_{i=1}^{m} \vec{F}_{iz}(r_{ij}) = \sum_{i=1}^{m}\sum_{j=1}^{n} F_z(r_{ij}) = 0 \end{cases} \quad (5)$$

i : numbers assigned to all the atoms of diamond cutters that affect the Morse force of a certain silicon atom.

j : numbers assigned to other silicon atoms inside the cut-off radius other than a certain silicon atom affected by the Morse force of cutter.

m : quantity of all the diamond cutter atoms when corresponding to a certain silicon atom affected by the Morse force of cutter.

n : quantity of other silicon atoms inside the cut-off radius other than a certain silicon atom affected by the Morse force of cutter.

r_{ij} : distance between the jth silicon atom in the silicon material and the corresponding ith atom of diamond cutter, and the distance between the jth silicon atom and the corresponding ith silicon atom.

To find the most suitable displacement position by optimization search method, it firstly has to define a searching range. Hooke-Jeeves search method is employed to carry out the search. First of all, the starting point has to be defined. In each cutting step, the silicon atom affected by the Morse force of the diamond cutter is the starting point of search. The increment of search is 0.001Å, and the convergence value $\varepsilon=10^{-4}$. The above logic is used to carry out the search of the most suitable displacement position point in each step, which is just our acceptable new point of force balanced displacement position.

Focusing on the nanoscale orthogonal cutting simulation of single-crystal silicon, this paper proposes the following methods. First of all, the new coordinates of atoms after displacement in each step are calculated. Then, the atoms are numbered. According to finite element method (FEM), segmented grids are arrayed and numbered one by one. Based

on these numbers, they are substituted in cut-off radius equation, Morse potential function, force balance as well as stress and strain equations in proper order. The calculated equivalent strain and Morse force are respectively substituted in the equations for calculation of plastic heat source and friction heat source. Adding temperature rise values of these two heat sources up, the temperature field distribution of single crystal silicon without heat transfer can be found.

B. Calculation of Equivalent Stress and Equivalent Strain

Using the shape function concept of finite element and the obtained the displacement of each atom, it can calculate the atomic-grade equivalent strain. Besides, after regression treatment of the flow stress-strain curve in nanoscale thin film tensile numerical experiment, the paper acquires flow stress-strain relational equation, which is also called flow curve. Using the flow curve, the paper calculates the equivalent stress produced from equivalent strain of element.

For the orthogonal nanocutting the single-crystal silicon workpiece, this study takes the equivalent strain and equivalent stress on the middle cross-section the single-crystal silicon after cutting of silicon workpiece, and ignore the effect in Z direction. Thus, the strain-displacement relational equation is as follows [12]:

$$\{\varepsilon\}=\begin{Bmatrix}\varepsilon_x\\ \varepsilon_y\\ \varepsilon_{xy}\end{Bmatrix}=\begin{Bmatrix}\dfrac{\partial u}{\partial x}\\ \dfrac{\partial v}{\partial y}\\ \dfrac{\partial u}{\partial x}+\dfrac{\partial v}{\partial y}\end{Bmatrix} \tag{6}$$

Therefore, for the displacement of each atom of the single-crystal silicon workpiece, the atomic grade equivalent strain can be obtained by using strain-displacement relational equation of continuum mechanics. Since strain-displacement relationship is purely a transformation of geometric relationship, instead of a relationship of mechanics, there should be no queries created. Therefore, after calculation of displaced position of atom at each step by molecular statics, the strain-displacement relational equation of macroscopic mechanics can be used to acquire the atomic grade equivalent strain. This paper supposes the position of the atom point as the node and uses the concept of shape function of finite element method.

Therefore, the strain-displacement relational equation of element is derived as follows [13]:

$$\therefore\{\varepsilon\}=\begin{Bmatrix}\varepsilon_x\\ \varepsilon_y\\ \varepsilon_{xy}\end{Bmatrix}=\frac{1}{2A}\begin{bmatrix}\beta_i & 0 & \beta_j & 0 & \beta_m & 0\\ 0 & \gamma_i & 0 & \gamma_j & 0 & \gamma_m\\ \gamma_i & \beta_i & \gamma_j & \beta_j & \gamma_m & \beta_m\end{bmatrix}\begin{Bmatrix}u_i\\ v_i\\ u_j\\ v_j\\ u_m\\ v_m\end{Bmatrix}=\{B\}\{\delta\} \tag{7}$$

where $\{\varepsilon\}$: strain matrix of element

$\{B\}$: displacement-strain relationship matrix

$\{\delta\}$: node displacement matrix.

It can be seen that that after the displacement components of single-crystal silicon atoms had been acquired from the quasi-steady nano-cutting model, the strain of the triangular element can be obtained from (7). Then, from the acquired strain of element made up of silicon atoms in the equation, the equivalent strain of element can be further calculated.

Regarding the equation for the relationship curve between equivalent strain and equivalent stress, this paper uses (8) of the equivalent stress-equivalent strain curve acquired from Aly et al. [14] simulation experiment of the numerical tensile value of nanoscale silicon film, as the basis. Then, the relationship curve between equivalent stress and equivalent strain required by the paper can be acquired. According to (8) and the equivalent strain calculated above, the equivalent stress produced under the equivalent strain of each element can be calculated.

$$\begin{aligned}\bar{\sigma}&=687.5043\bar{\varepsilon}^3-490.9562\bar{\varepsilon}^2+148.4096\bar{\varepsilon}+7.7323 && \bar{\varepsilon}\le 0.25\\ \bar{\sigma}&=46.2108\bar{\varepsilon}+13.8598 && \text{else}\end{aligned} \tag{8}$$

C. Calculation of Temperature Rise Without Considering Heat Transfer of Cutting Single-Crystal Silicon

This paper carries out quasi-steady molecular statics simulation in three-dimensional way, and the initial temperature of workpiece and cutting tool are both supposed to be at room temperature (298K). However, the cutting state is orthogonal cutting, and is in symmetric shape in Z direction of the workpiece width. Thus, this paper neglects the heat transfer effect on Z axis, and only explores the temperature distribution on the cross-section near the center in X and Y directions.

In the nanocutting process, this paper supposes that the main heat is produced from two heat sources as follows:

1. Plastic deformation heat produced from quasi-plastic deformation, which is caused by deformation between atoms of workpiece.
2. Friction heat produced between workpiece atoms and tool atoms.

This paper applies the equivalent strain calculated by the three-dimensional quasi-steady molecular statics nanocutting simulation model developed by this paper, and then substitutes it in the flow-stress curve to obtain equivalent stress. Multiplying the equivalent stress by the equivalent strain, the heat produced by the plastic heat source of quasi-plastic deformation can be acquired. Besides, applying the calculation method of nanocutting force with the use of quasi-steady molecular statics nanocutting model, this paper can acquire the force balance of Morse force and the instant displacement increment of workpiece atoms. With the concept of force balance, the total Morse force borne by the copper workpiece atoms in contact with the tool face can be decomposed to be component force in X, Y and Z directions. Furthermore, the Morse force borne by each workpiece atom being close to the tool face is decomposed to be normal component force and tangential component force on the tool face. The component force in tangential direction is just the force similar to friction force produced by cutting of workpiece. The product of multiplying the friction force borne by atoms by the

displacement of atoms along the tangential side of cutting tool can be regarded as the friction heat produced by the quasi-friction of workpiece atoms on the tool face.

Currently, towards solving the problems of nanocutting, most people commonly use three-dimensional molecular dynamics to solve the cutting temperature field. To solve the chips and temperature distribution inside the workpiece, there is still no one using the concept of combining quasi-steady molecular statics nanocutting simulation model with the heat source mentioned above in this paper.

This paper supposes that in the workpiece atoms in contact with the tool face, friction heat is produced in the various atoms with the adjacent distance between the workpiece atoms bearing Morse force and the tool atoms being smaller than 1 Å. Therefore, Δd_{fi} is supposed to be the displacement increment of workpiece atoms on the tool face in tangential direction. Thus, $\Delta d_{fi} = v_{fi}\Delta t$.

As mentioned above, friction heat is supposed to be produced from the friction between the atoms on cutting tool and the workpiece atoms. The calculation method of frication heat is shown as follows:

$$Q_{fi} = \frac{F_{fi} v_{fi} \Delta t}{J} = \frac{F_{fi} \Delta d_{fi}}{J} \tag{9}$$

where F_{fi} : friction force on the tool face after decomposing the Morse force borne by workpiece atoms.

v_{fi} : tangential speed of the interface between workpiece atoms and the tool face atoms.

Δt : time interval.

For the product of multiplying the equivalent stress by equivalent strain of each element obtained in the nanocutting simulation model, this paper regards it as quasi-plastic heat source. Therefore, within the time Δt of workpiece, this paper supposes that the temperature rise caused by quasi-plastic deformation is:

$$\Delta T_d = \frac{\int \bar{\sigma}\,\dot{\bar{\varepsilon}}\,\Delta t}{Jc\rho} \tag{10}$$

where c denotes the specific heat, and ρ denotes the density of material.

Since the abovementioned friction heat is produced on the various workpiece atoms contacting along the tool face direction, they are distributed to the nearest cutting tool and workpiece atoms in α_w/α_t proportion. Thus, the temperature rise distributed to the workpiece and the tool face are ΔT_{wi} and ΔT_{ti} respectively, being (11) as follows [15]:

$$\begin{aligned} \Delta T_{wi} &= \frac{\alpha_w}{\alpha_w + \alpha_t} \frac{1}{c_w \rho_w v_w} Q_{fi} \\ \Delta T_{ti} &= \frac{\alpha_t}{\alpha_w + \alpha_t} \frac{1}{c_t \rho_t v_t} Q_{fi} \end{aligned} \tag{11}$$

where $\alpha_w = \left(\frac{k_w}{c_w \rho_w}\right)^{\frac{1}{2}}$, $\alpha_t = \left(\frac{k_t}{c_t \rho_t}\right)^{\frac{1}{2}}$

In the equation, v_w and v_t are the volume of particles on the interface of workpiece and cutting tool respectively, whereas k_w and k_t are the thermal conductivity coefficients of workpiece and cutting tool respectively.

III. Finite Difference Equation of Heat Transfer And Calculation of Temperature Field After Heat Transfer

The heat sources produced by plastic deformation and friction respectively are supposed to appear at the beginning moment of each simulation step, and then are evenly transferred within the time Δt. Under the condition that Δt is very small, the above supposition is considered reasonable. In this way, the above heat transfer phenomenon is considered a transient heat transfer problem. As it mentioned above, this paper neglects the heat transfer effect on axis, and only explores the temperature distribution on the cross-section near the center in X and Y direction. The Cartesian coordinate partial differential heat transfer equation is:

$$\frac{\partial T}{\partial t} = \alpha \left(\frac{\partial^2}{\partial x^2} + \frac{\partial^2}{\partial y^2} \right) T \tag{12}$$

where $\alpha = \frac{k_c}{\rho c}$, being called thermal diffusivity, and k_c is thermal conductivity coefficient (supposed to be $k_x = k_y = k_z$ in this paper).

In the cutting process, there is a slight difference in heat transfer way between the internal element and the boundary element of workpiece. Related description is separately made on the internal element and the boundary elements:

A. Internal Element

The heat transfer elements in simulation process are quadrilateral elements. Thus, the so-called "internal element" just refers that the heat transfer element is adjacent to four heat transfer elements at its four sides, without thermal convection and thermal radiation, as shown in Fig. 1. Using central difference method, (12) can be written in a finite difference form as follows [15]:

$$T_{i,j}^{p+1} = \alpha \Delta t \left[\frac{T_{i+1,j}^{p} + T_{i-1,j}^{p}}{(\Delta x)^2} + \frac{T_{i,j+1}^{p} + T_{i,j-1}^{p}}{(\Delta y)^2} \right] \left\{ 1 - 2\alpha \Delta t \left[\frac{(\Delta x)^2 + (\Delta y)^2}{(\Delta x)^2 (\Delta y)^2} \right] \right\} T_{i,j}^{p} \tag{13}$$

B. Boundary Element

The so-called "boundary element" refers that the number of heat transfer elements around the boundary element is not as many as four, and that it is adjacent to air. Therefore, this simulation considers thermal convection, but does not consider thermal radiation. As shown in Fig. 1, the central heat transfer element is (i, j), the surface in $(i, j+1)$ direction contacts with air to undergo thermal convection, and the value of $T_{i,j+1}^{p}$ is T_{∞}. Then the heat transfer [15] is:

$$T_{i,j}^{p+1} = T_{i,j}^{p} + \frac{\Delta t}{\rho c \Delta x \Delta y} \left[k_c \cdot \frac{T_{i+1,j}^{p} - T_{i,j}^{p}}{\Delta x} \cdot \Delta y + k_c \cdot \frac{T_{i,j-1}^{p} - T_{i,j}^{p}}{\Delta y} \cdot \Delta x + k_c \cdot \frac{T_{i+1,j}^{p} - T_{i,j}^{p}}{\Delta x} \cdot \Delta y + h_c \cdot \Delta x \cdot (T_{\infty} - T_{i,j}^{p}) \right] \tag{14}$$

In (13) and (14), k_c is the thermal conductivity, α is the thermal diffusivity and h_c is the heat transfer coefficient for convection.

The symbols in (13) correspond to those in Fig. 1 (a), and the symbols in (14) correspond to those in Fig. 1 (b). In the equations, $T^p_{i-1,j}$, $T^p_{i,j}$, $T^p_{i+1,j}$, $T^p_{i,j-1}$ and $T^p_{i,j+1}$ are the initial temperatures of the quadrilateral elements (i, j), $(i+1, j)$, $(i-1,j)$, $(i,j+1)$ and $(i,j-1)$ respectively in each incremental deformation step. Δx and Δy denote the distance of any two quadrilateral elements in horizontal direction and vertical direction respectively. Δt denotes the time increment. $T^{p+1}_{i,j}$ denotes the temperature of element (i,j) within the time Δt after heat transfer.

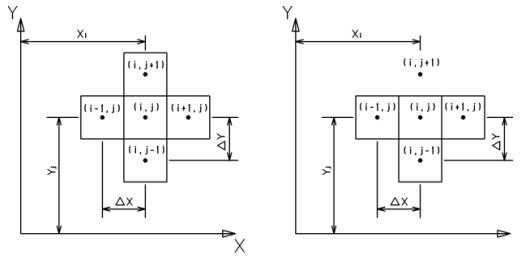

Fig. 1 Diagrams of (a) internal element and (b) boundary element for heat transfer

There is one thing noteworthy about heat transfer finite difference equation that the heat source items on the right hand side of (13) and (14) disappear. The reason for this is that the heat source derived from plastic deformation of workpiece has been pre-treated by (10) and (11) before heat transfer, and then transformed to be the corresponding temperature rise ΔT_d, ΔT_w and ΔT_t. Therefore, the heat source items of the paper are no longer added to (13) and (14).

After heat analysis is made above, nanocutting simulation can be carried out. In Step One, the initial temperatures of workpiece and cutting tool are both supposed to be room temperature (298K). After the cutting tool starts to cut in the workpiece, the cutting tool moves forward by the way of incremental displacement. During this period, the initial temperatures are substituted in the heat transfer difference, namely (13) and (14), acquiring the results of temperature distribution on workpiece after heat transfer. Then the plastic deformation of workpiece as well as the heat source derived from the interface friction between workpiece and cutting tool can be obtained. Using (9) to (11), the above two heat sources are transformed to be the corresponding temperature rise ΔT_d, ΔT_w and ΔT_t. If the above temperature is regarded to be happened at the beginning moment of next step, it would be added to the temperature distribution result of the corresponding atoms of workpiece after heat transfer in previous step, and the initial temperatures of workpiece and cutting tool in next step can be acquired. After that, the cutting tool moves forward again by the way of incremental displacement. Similarly, these temperatures are substituted in the heat transfer finite difference equations, achieving the temperature distribution results of silicon workpiece after heat transfer. Then, the cutting tool moves forward continuously by the way of incremental displacement. The above treatment process repeats all the time until steady-state cutting is achieved. After the above steps, calculation is made, and it can acquire the temperature distribution results of silicon workpiece and chips after heat transfer.

IV. Results and Discussion

A. Construction of Simulation Model

During cutting, although the hardness of silicon material is very high, it is considered relatively soft when compared to diamond cutting tool. Therefore, diamond cutting tool is considered a rigid body during simulation. When the distance between two atoms reaches $2.5r_c$, potential function is almost equal to zero. Hence, this paper takes $2.5r_c$ as the cut-off radius. The simulated workpiece is divided into free movement zone and fixed boundary zone. The layer of atoms by the left side of workpiece material and the two layers of atoms at the bottom of workpiece material are fixed and not moved. All other atoms can be affected by cutting tool, and deformation and mobility would be caused.

This paper carries out nanoscale orthogonal cutting simulation for single crystal silicon workpiece by two cutting tools in different shapes. The first cutting tool is a round-edge tip with nose radius 5Å, clearance angle 10° and rake angle 15°, and the second cutting tool, its front sharp end part is modified to be a round-edge tip with nose radius 5Å, clearance angle 10° and rake angle -15°.

Regarding the simulation, different cutting tools conduct orthogonal cutting silicon workpiece, and comparison is subsequently made. The three following simulation cases are used to make further analysis. The each workpiece is single crystal silicon with a width of four lattices. Fig. 2 shows the initial simulation diagram of the relative positions of the cutting tools and silicon workpiece. Table I shows the orthogonal cutting parameters during simulation set by this paper.

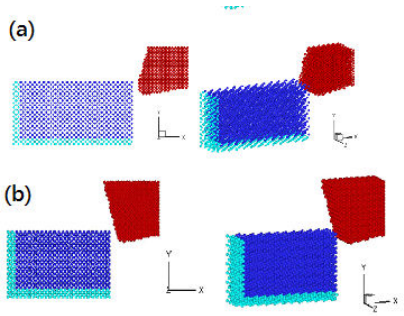

Fig. 2 Diagram of initial conditions of different simulation examples (a) Round edge diamond cutter with nose radius of 5Å, rake angle of 15° (b) Round edge diamond cutter with nose radius of 5Å, rake angle of -15°

TABLE I
COMPUTATIONAL PARAMETERS OF ORTHOGONAL NANOCUTTING A SINGLE CRYSTAL SILICON WORKPIECE

Work material	12a × 6a × 4a atoms:2615 (width of 4 lattices is 21.72 Å)	
Lattice constant of silicon	a=5.431 Å	
Feeding step	0.002 Å	
Total feeding step	50 Å	
Depth of cutting	6.43Å	
Tool	Rigid-body diamond	
Tip radius	5 Å	
Clearance angle of tool	10°	
Rake angle of tool	15°	-15°
Total tool atoms	2968	3780

B. Analysis of Cutting Force in Orthognal Nanocutting the Single-Crystal Silicon Workpiece

When exploring cutting force, it defines that the mutual attraction force between diamond cutting tool and single-crystal silicon workpiece during cutting is a negative value, and the repulsive force between them is a positive value. Fig. 3 shows the numerical diagram of orthogonal cutting force and thrust force acquired from simulation of orthogonal cutting a silicon workpiece by a round-edge cutting tool with rake angle 15°, clearance angle 10° and nose radius 5Å. Since the contact area between silicon workpiece and the round-edge tip is greater than that between the silicon workpiece and the tip of the sharp cutting tool, the numerical value of cutting force made by the round-edge cutting tool in Fig. 4 is a greater than that of cutting force made by the sharp-edge cutting tool in Fig. 3. The stable numerical value of cutting force is around 53nN and the stable numerical value of thrust force is around 32nN.

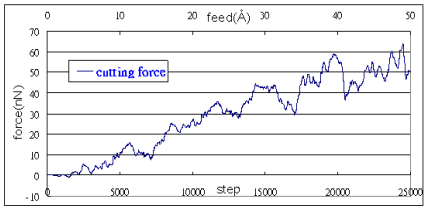

(a) Cutting force

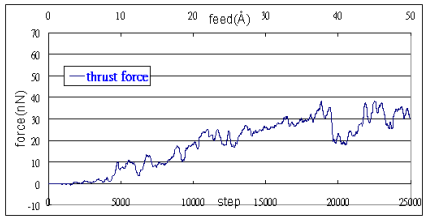

(b) Thrust force

Fig. 3 The numerical diagram of cutting force and thrust force acquired from simulation of orthogonal cutting a silicon workpiece by a round-edge cutting tool with rake angle 15°, clearance angle 10° and nose radius 5Å

Fig. 4 shows the numerical diagram of orthogonal cutting force and thrust force acquired from simulation of orthogonal cutting a silicon workpiece by a round-edge cutting tool with rake angle -15°, clearance angle 10° and nose radius 5Å. Since the contact area between silicon workpiece and the round-edge tip is greater than that between the silicon workpiece and the tip of the sharp cutting tool, the numerical value of cutting force made by the round-edge cutting tool in Fig. 5 is a greater than that of cutting force made by the sharp-edge cutting tool in Figs. 3 and 4. The stable numerical value of cutting force is around 62nN and the stable numerical value of thrust force is around 39nN.

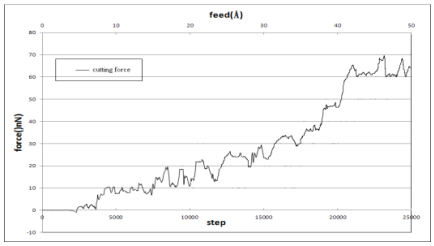

(a)Cutting force

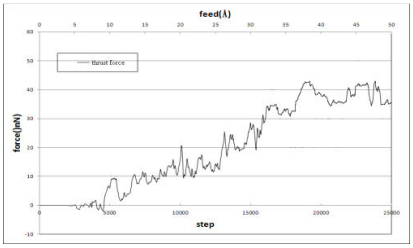

(b) Thrust force

Fig. 4 shows the numerical diagram of cutting force and thrust force acquired from simulation of orthogonal cutting a silicon workpiece by a round-edge cutting tool with rake angle -15°, clearance angle 10° and nose radius 5Å

In Table II, it summarizes the average stable numerical values of cutting forces and thrust forces acquired from simulation of orthogonal cutting by three different cutting tools.

TABLE II
AVERAGE STABLE NUMERICAL VALUES OF CUTTING FORCES AND THRUST FORCES ACQUIRED FROM SIMULATION OF ORTHOGONAL CUTTING A SINGLE-CRYSTAL SILICON WORKPIECE BY DIFFERENT DIAMOND CUTTING TOOLS

	Orthogonal cutting force (nN)	Thrust force (nN)
Sharp-edge cutting tool with rake angle 15°	50	28
Round-edge cutting tool with rake angle 15°	53	32
Round-edge cutting tool with rake angle -15°	62	39

C. Analysis of Equivalent Strain and Equivalent Stress in Orthogonal Nanocutting Single -Crystal Silicon Workpiece

Using this paper's calculation method of equivalent stress and equivalent strain mentioned above, this paper calculates the equivalent strain and equivalent stress on the middle cross-section of workpiece after cutting the silicon workpiece. In order to know the distribution of equivalent strain and equivalent stress, it draws the distribution curve diagram of equivalent strain and equivalent stress on the middle

cross-section of the cut single-crystal silicon workpiece at the 20,000th step, as shown in Fig. 5 and Table III.

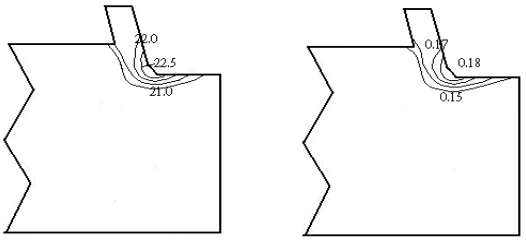

(a) Equivalent stress (b) Equivalent strain

Fig. 5 shows the diagram of equivalent stress and equalent strain acquired from simulation of orthogonal cutting of a single-crystal silicon workpiece by a round-edge cutting tool with rake angle -15°, clearance angle 10° and nose radius 5Å

TABLE III
NUMERICAL VALUES OF MAXIMUM EQUIVALENT STRESS AND MAXIMUM EQUIVALENT STRAIN ACQUIRED FROM CUTTING SIMULATION OF SINGLE-CRYSTAL SILICON WORKPIECE BY DIFFERENT DIAMOND TOOLS

	Maximum equivalent Stress $\bar{\sigma}$ (GPa)	Maximum equivalent Stress $\bar{\varepsilon}$
Round-edge cutting tool with rake angle 15°	21.5	0.16
Round-edge cutting tool with rake angle -15°	22.5	0.18

From Table III, it is known that the maximum equivalent stress and maximum equivalent strain acquired from simulation of cutting by a tool with smaller rake angle are greater, and that the maximum equivalent stress and maximum equivalent strain acquired from simulation of cutting by the round edge tool with edge radius are greater than those by the sharp edge tool.

D. Verification and Comparison of Temperature Distribution of the Silicon Workpiece after Nanoscale Orthogonal Cutting a Single-Crystal Silicon Workpiece

In order to verify the applicability of the quasi-steady molecular statics nanocutting model for simulating temperature field of silicon workpiece developed by this paper, this paper further applies the abovementioned feasibility of the theoretical model for calculation temperature rises caused by plastic heat source and friction heat source induced by cutting a single crystal silicon workpiece. This paper sets the cutting tool to be a round-edge diamond cutting tool with rake angle 15° and nose radius 5Å. The cutting tool simulates cutting a single-crystal silicon workpiece with width 21.72Å (width of 4 lattices) at the cutting depth 6.43Å. Qualitative comparison is made between the simulation results of temperature in numerical values and the cutting temperature distribution indicated by Cai et al. in [10]. Cai et al. [10] used molecular dynamics to conduct simulation and calculate the cutting temperature distribution of single-crystal silicon workpiece. From this paper's simulation results of temperature field of cutting a single-crystal silicon workpiece, it can be found that after the 20,000th step, the values are nearly in steady state. Therefore, as acquired from the diagram of numerical values of temperature and temperature distribution at the 20,000th step, the highest temperature without heat transfer of atoms on single-crystal silicon chips is around 859K and the highest temperature with heat transfer is around 812k.; the higher temperature of the single-crystal silicon workpiece close to the tip area of cutting tool is at the range of 700~850K as shown in Figs. 6 (a) and (b); and the temperature of silicon workpiece around the tip zone area of cutting tool acquired by Cai et al. [10] was around 725K. The temperature calculated by Cai et al. [10] was zonal temperature, but the data of zonal temperature calculated by this study has a certain difference from the data of the above reference. However, they are closer to the rough numerical value of temperature distribution and it is acceptable qualitatively.

The difference between the values of this paper and those of Cai et al. [10] may be caused by the greater nose radius of Cai's [10] cutting tool and its greater cutting depth adopted. Besides, the molecular dynamics cutting simulation model employed by Cai et al. [10] is different from this paper's quasi-steady molecular statics nanocutting simulation model used for calculation of temperature. The calculation of cutting temperature by using molecular dynamics is conversion of the kinetic energy of atom under high-speed motion to be heat source. Regarding the method of using molecular statics for calculation of cutting temperature in this study, it calculates the temperature rises of two kinds of heat sources: plastic deformation heat and friction heat of atom on the tool face. But in [10], Cai et al. did not consider that the friction heat of atom on the tool face would be distributed to the cutting tool, as mentioned in (13). Therefore, the results calculated in this study are different from the numerical value of cutting temperature obtained by Cai et al. [10], but they are still close to Cai's values of temperature distribution of [10] qualitatively. Therefore, it is qualitative verified that the orthogonal nanocutting simulation results of this study is reasonable and the three dimension quasi-steady molecular statics nanocutting model for calculating temperature field of silicon workpiece may be acceptable.

E. Analysis of Temperature Distributions of Single-Crystal Silicon Workpiece and the Cut Workpiece's Temperature Rise Caused by Plastic Heat Source and Friction Heat Source

Using the above mentioned calculation methods of plastic heat source, friction heat source and temperature rises with applying the temperature simulation model of quasi-steady molecular statics nanoscale cutting, and the initial temperature of workpiece and cutting tool are both supposed to be at room temperature (298K), this paper calculates the temperature produced from plastic heat source on the middle cross-section and the temperature rise produced from friction heat source after cutting silicon workpiece. This paper also adds the total temperature rise produced from plastic heat source with the total temperature rise produced from friction heat source and room temperature when steady cutting force is reached. It also calculates the final temperatures without heat transfer and with heat transfer of single-crystal silicon workpiece during nanoscale orthogonal cutting. After that, contour lines are drawn to indicate the temperature field distribution curve

diagram on the middle cross-section of the single-crystal silicon workpiece being cut.

The cutting simulation from the 20,000th to 25,000th step is more stable, so that this paper selects the cutting of the 20,000th step to observe the temperature field distribution trend on the middle cross-section of a single-crystal silicon workpiece. Fig. 6 shows the diagram of temperature field of a silicon workpiece cut by a round-edge cutting tool with rake angle 15°, clearance angle 10° and nose radius 5Å. The highest temperature after heat transfer produced is around 812K. Fig. 7 shows the diagram of temperature field of a silicon workpiece cut by a round-edge cutting tool with rake angle -15°, clearance angle 10° and nose radius 5Å. The highest temperature after heat transfer produced is around 844K. As known from Fig. 6 and Fig. 7, when the silicon workpiece is being cut, the heat source temperature is concentrated on the chips contacting the tip area of the cutting tool. And higher temperature and larger high temperature zone are produced during cutting by the negative rake angle cutting tool than that by the positive one. Perhaps this is because the nose tip area of the negative rake angle cutting tool is greater than the tip area of the positive rake angle cutting tool. Besides, the highest temperature without heat transfer is higher than that after heat transfer. Besides, the cutting force, thrust force, equivalent stress and equivalent strain are greater during cutting by the negative rake angle cutting tool, leading to greater plastic deformation heat and friction heat and greater temperature rises.

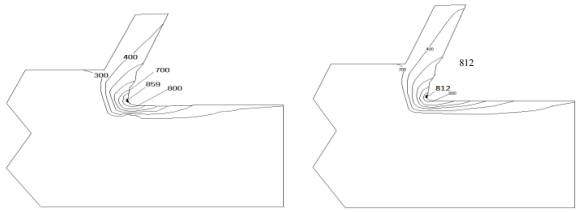

(a) (b)

Fig. 6 The diagram of temperature field of a silicon workpiece cut by a round-edge cutting tool with rake angle 15°, clearance angle 10° and nose radius 5Å, (a) without consideration of heat transfer, and (b) with consideration of heat transfer

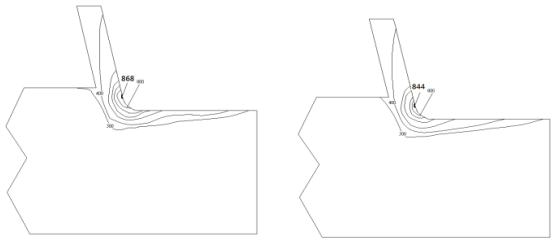

(a) (b)

Fig. 7 The diagram of temperature field of a silicon workpiece cut by a round-edge cutting tool with rake angle -15°, clearance angle 10° and nose radius 5Å, (a) without consideration of heat transfer, and (b) with consideration of heat transfer

First of all, this paper calculates the Morse force of atom on the middle cross-section of silicon workpiece contacting the cutting tool, and then decomposes Morse force to be the force in tangential direction along the tool face and the normal force vertical to the tool face. The force in tangential direction along the tool face is just the friction force during the contact between silicon atom and cutting tool. Selecting the diagram on the middle cross-section of silicon workpiece when being cut to the 20,000th step, this paper lists out the calculated friction forces of the silicon atoms contacting the tool face in a table to make analysis.

Fig. 8 shows the diagram on the middle cross-section of a silicon workpiece cut by a round-edge cutting tool with rake angle 15°, clearance angle 10° and nose radius 5Å. In Fig. 8, the numbered atoms are the silicon atoms contacting the tool face. Table IV shows the temperature rise ($\Sigma\Delta Td$) caused by plastic heat source and temperature rise ($\Sigma\Delta Tw$) caused by friction heat source, as well as the total temperature rise ($\Sigma\Delta T$) of the cut silicon workpiece atoms at the 20000th step in Fig. 8. As known from Table IV, for No. 3 atom, its temperature rise caused by plastic heat source is 509K, its temperature rise caused by friction heat source is 52K, and the total temperature rise is the greatest, around 561K, thus the final temperature without heat transfer for No.3 atom is 859K and the final temperature after heat transfer is 812K in Table IV shown. Table V shows the normal force produced from the atoms contacting the tool face, as indicated in Fig. 8, as well as the friction force in tangential direction. As known from Table V, the friction force of atom No. 3 is the greatest, being around 19 nN and it also shown that the ΔT_w of atom No.3 is the greatest. Fig. 9 shows the diagram on the middle cross-section of a silicon workpiece cut by a round-edge cutting tool with rake angle -15°, clearance angle 10° and nose radius 5Å. In Fig. 9, the numbered atoms are the silicon atoms contacting the tool face. Table VI shows the temperature rise ($\Sigma\Delta T_d$) caused by plastic heat source and temperature rise ($\Sigma\Delta T_w$) caused by friction heat source, as well as the total temperature rise ($\Sigma\Delta T$) of the cut silicon workpiece atoms at the 20000th step in Fig. 9. As known from Table VI, for No. 4 atom, its temperature rise caused by plastic heat source is 529K, its temperature rise caused by friction heat source is 59K, and the total temperature rise is the greatest, around 588K, thus the final temperature without heat transfer for No. 4 atom is 868K and the final temperature after heat transfer is 844K in Table VI shown. Table VII shows the normal force produced from the atoms contacting the tool face, as indicated in Fig. 7, as well as the friction force in tangential direction. As known from Table VII, the friction force of atom No. 4 is the greatest, being around 42 nN and it also shown that the ΔT_w of atom No.4 is the greatest. As seen from the numerical comparison between Table V and Table VII, the friction forces of workpiece atoms during cutting by the negative rake angle cutting tool is greater than the tip area of the positive rake angle cutting tool. Therefore, the temperature rise (ΔT_w) caused by friction heat during cutting by a negative rake angle cutting tool is also greater.

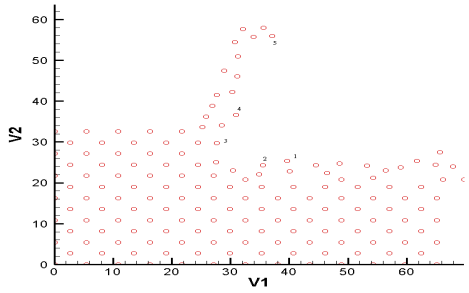

Fig. 8 The diagram on the middle cross-section of a silicon workpiece cut by a round-edge cutting tool with rake angle 15°, clearance angle 10° and nose radius 5Å (at the 20,000th step)

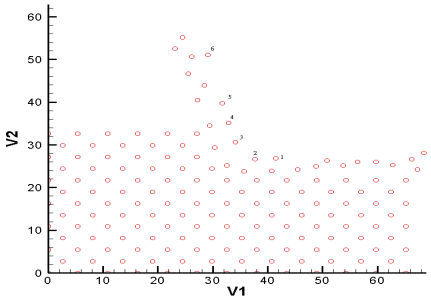

Fig. 9 The diagram on the middle cross-section of a silicon workpiece cut by a round-edge cutting tool with rake angle -15°, clearance angle 10° and nose radius 5Å (at the 20,000th step)

TABLE IV
TEMPERATURE RISE DURING CUTTING BY A ROUND-EDGE CUTTING TOOL WITH RAKE ANGLE 15° (AT THE 20000TH STEP)

No. of atom	The total temperature rise by the plastic deformation heat $\Sigma\Delta T_d$ (K)	The total temperature rise by the frictional heat $\Sigma\Delta T_w$ (K)	The total temperature rise $\Sigma\Delta T$ (K)	The total temperature rise after heat transfer $\Sigma\Delta T_f$ (K)	The final temperature without heat transfer (K)	The final temperature after heat transfer (K)
1	365	32	397	362	695	660
2	461	43	504	459	802	757
3	509	52	561	514	859	812
4	346	42	388	355	686	653
5	108	25	133	105	431	408

TABLE V
THE FORCE, DISPLACEMENT AND TEMPERATURE RISE CAUSED BY FRICTION HEAT SOURCE FOR SILICON ATOMS CUT BY A ROUND-EDGE CUTTING TOOL WITH RAKE ANGLE 15° DURING CONTACT WITH THE TOOL FACE (AT THE 20000TH STEP)

No. of atom	The displacement on the surface of the tool (Å)	The normal force on the surface of the tool (nN)	The friction force on the surface of the tool (nN)	ΔTw(K) at the 20000th step
1	0.00052	36.32	9.73	0.083
2	0.00186	21.85	13.18	0.402
3	0.00174	35.65	19.67	0.561
4	0.00122	18.88	18.88	0.378
5	0.00104	56.22	15.07	0.256

TABLE VI
TEMPERATURE RISE DURING CUTTING BY A ROUND-EDGE CUTTING TOOL WITH RAKE ANGLE -15° (AT THE 20000TH STEP)

No. of atom	The total temperature rise by the plastic deformation heat $\Sigma\Delta T_d$ (K)	The total temperature rise by the frictional heat $\Sigma\Delta T_w$ (K)	The total temperature rise $\Sigma\Delta T$ (K)	The total temperature rise after heat transfer $\Sigma\Delta T_f$ (K)	The final temperature without heat transfer. (K)	The final temperature after heat transfer. (K)
1	333	44	377	343	675	641
2	439	47	486	449	784	747
3	470	50	520	480	818	778
4	529	59	588	546	868	844
5	299	42	341	310	639	608
6	116	29	145	120	443	418

As seen from Figs. 8 and 9, Tables V and VII, the greatest friction forces all happen to the places a little bit close to the area of tip zone. And after heat transfer, the total temperature rise of the cut workpiece atoms in contact with the tool surface would all fall. This is because the temperature of the cut workpiece atoms in contact with the tool surface is higher. In the process of heat transfer, heat source temperature is transferred to the adjacent atoms with lower temperature, making the temperature of the cut workpiece atoms in contact with the tool surface fall slightly.

TABLE VII
THE FORCE, DISPLACEMENT AND TEMPERATURE RISE CAUSED BY FRICTION HEAT SOURCE FOR SILICON ATOMS CUT BY A ROUND-EDGE CUTTING TOOL WITH RAKE ANGLE -15° DURING CONTACT WITH THE TOOL FACE (AT THE 20000TH STEP)

No. of atom	The displacement on the surface of the tool (Å)	The normal force on the surface of the tool (nN)	The friction force on the surface of the tool (nN)	ΔTw(K) at the 20000th step
1	0.00157	58.21	28.64	0.738
2	0.00177	42.83	23.29	0.674
3	0.00122	36.60	36.60	0.734
4	0.00132	16.97	41.96	0.905
5	0.00155	24.12	24.09	0.613
6	0.00141	22.98	22.94	0.531

V. CONCLUSION

This paper uses three-dimensional quasi-steady molecular statics nanoscale orthogonal cutting model to carry out simulation of cutting of silicon material. According to the simulation results, this paper finds that the temperature rise of the cut workpiece caused by plastic heat source is greater than the temperature rise caused by friction heat source. Hence, the temperature rise of the cut workpiece mainly comes from the temperature rise of plastic deformation. After heat transfer, the total temperature rise of the cut workpiece atoms in contact with the tool surface would fall. This is because the temperature of the cut workpiece atoms in contact with the tool surface is higher. In the process of heat transfer, the heat source temperature is transferred to the adjacent atoms with lower temperature, making the temperature of the cut workpiece atoms in contact with the tool surface fall slightly.

ACKNOWLEDGMENT

The authors would like to give special thanks to the National Science Council, Taiwan, for financial support through Contract No. NSC 99-2221-E-011-019.

REFERENCES

[1] S. Shimada, "Molecular Dynamics Analysis as Compared with Experimental Results of Micromachining," *Ann. CIRP*, vol.41, no. 1, pp.117-120, 1990.
[2] T. H. C. Childs and K. Maewaka, "Computer-aided Simulation and Experimental Studies of Chip Flow and Tool Wear in the Turning of Flow Alloy Steels by Cemented Carbide Tools" ,*Wear*, vol. 139, no.2, pp.235-250, 1990.
[3] J. Belak, and I. F. Stowers, "A Molecular Dynamics Model of the Orthogonal Cutting Process," *Proc. Am. Soc*., *Precision Eng.*, pp.76-79, 1990.
[4] Q. X. Pei, C. Lu, F. Z. Fang and H. Wu, "Nanometric Cutting of Copper: A Molecular Dynamics Study," *Computational Materials Science*, pp.434-441, 2006.
[5] T. Inamura, N. Takezawa and, Y. Kumaki, "Mechanics and Energy Dissipation in Nanoscale Cutting", *Annals. CIRP*, vol.42, no.1, pp.79-82,1993.
[6] M. B. Cai, X. P. Li, M. Rahman, " Study of the Mechanism of Nanoscale Ductile Mode Cutting of Silicon Using Molecular Dynamics Simulation" ,*International Journal of Machine Tool & Manufacture* pp.75-80, 2007.
[7] S. Shimada, "Molecular Dynamics Analysis of Nanometric Cutting Process", *Ann. CIRP*, vol.29, no.283, pp.6, 1995.
[8] H. Tanaka1, S. Shimada, "Requirements for Ductile-mode Machining Based on Deformation Analysis of Mono-crystalline Silicon by Molecular Dynamics Simulation", *Annals of the CIRP*, vol.56, p53-56, 2007.
[9] Q. H. Tang, "MD Simulation of Dislocation Mobility During Cutting with Diamond Tip on Silicon", *Materials Science in Semiconductor Processing*, vol.10 , pp.270-275, 2007.
[10] M. B. Cai, X. P. Li, M. Rahman, "Study of the Temperature and Stress in Nanoscale Ductile Mode Cutting of Silicon Using Molecular Dynamics Simulation", *Journal of Materials Processing Technology*, 192–193 pp.607–612, 2007.
[11] L. A. Girifalco and V. G. Weizer, "Application of the Morse Potential Function to Cubic Metals," *Phys. Rev.*, vol. 114, pp. 687-690, 1959.
[12] J. H. L. The and R. F. Scrutton, "A Theoretical Analysis of Temperature Distributions in the Hight Speed Forging of Hot Steel, " *Trans. ASME, J. Enging. Materials and Technology*, vol.114, pp.218-226, 1992.
[13] Z. C. Lin, and J. C. Huang , "3D Nano-scale Cutting Model for Nickel Material," *Journal of Materials Processing Technology*, pp.27–36 , 2007.
[14] M. F. Aly, E. Ng, , S. C. Veldhuis, and M. A. Elbestawi, , "Prediction of Cutting Forces in the Micro-machining of Silicon Using a Hybrid Molecular Dynamic-finite Element Analysis Force Model," *International Journal of Machine Tool & Manufacture*, pp.1729-1737, 2007.
[15] Z. C. Lin, W. C.Pan, and S. P. Lo, "A Study of Orthogonal Cutting with Tool Flank Wear and Sticking Behavior on the Chip-Tool Interface," *Journal of Materials Processing Technology*, vol.52, no.2-4, pp.524-538, 1995.